

# Elucidation of the disulfide folding pathway of hirudin by a topology-based approach

C. Micheletti<sup>1</sup>, V. De Filippis<sup>2</sup>, A. Maritan<sup>1</sup> and F. Seno<sup>3</sup>,

<sup>1</sup>International School for Advanced Studies, via Beirut 2-4, 34014 Trieste, Italy, INFM and The Abdus Salam Centre for Theoretical Physics

<sup>2</sup>Dipartimento di Scienze Farmaceutiche and CRIBI Biotechnology Centre, Via Marzolo 5, University of Padova, 35131 Italy

<sup>3</sup> INFM-Dipartimento di Fisica ‘G. Galilei’, Via Marzolo 8, Università di Padova, 35131 Padova, Italy

(Dated: August 14, 2018)

A theoretical model for the folding of proteins containing disulfide bonds is introduced. The model exploits the knowledge of the native state to favour the progressive establishment of native interactions. At variance with traditional approaches based on native topology, not all native bonds are treated in the same way; in particular, a suitable energy term is introduced to account for the special strength of disulfide bonds (irrespective of whether they are native or not) as well as their ability to undergo intra-molecular reshuffling. The model thus possesses the minimal ingredients necessary to investigate the much debated issue of whether the re-folding process occurs through partially structured intermediates with native or non-native disulfide bonds. This strategy is applied to a context of particular interest, the re-folding process of Hirudin, a thrombin-specific protease inhibitor, for which conflicting folding pathways have been proposed. We show that the only two parameters in the model (temperature and disulfide strength) can be tuned to reproduce well a set of experimental transitions between species with different number of formed disulfide. This model is then used to provide a characterisation of the folding process and a detailed description of the species involved in the rate-limiting step of Hirudin refolding.

## INTRODUCTION

The characterisation of the folding pathway of proteins is one of the fundamental problems in molecular biology and is under an increasing scientific attention due to the continuous advancements in experimental and theoretical biochemistry. After the work of Anfinsen[1], who demonstrated that ribonuclease unfolds and refolds reversibly into its native (active) three-dimensional structure, it has generally been accepted that the primary sequence usually contains sufficient information to direct the complete folding process. What typically remains elusive to experimental and theoretical investigations is the pathway of this spontaneous process and the mechanisms that govern it.

A considerable progress in this direction is possible for proteins containing native disulfide bonds. The formation of disulfide bonds during the folding process can be controlled experimentally through the use of an appropriate thioldisulfide redox couple and thiol quenching agent[2, 3, 4]. By these means the regeneration process can be halted, the intermediate species can be trapped, isolated and characterised. Historically, one of the most investigated proteins containing disulfide bonds has been the bovine pancreatic trypsin inhibitor (BPTI). Starting with the work of Creighton [5] a series of crucial studies have accumulated a wealth of evidence in favour of the existence of partially structured intermediates along the protein folding pathway. Despite these efforts, the detailed characterisation of the intermediates turned out to be a delicate experimental matter and there is still not a universal agreement on whether intermediates contain native or non-native disulfide bonds[3, 4, 6] and if there exists more than one pathway[4, 7]. In this context, the use of theoretical and computational tools [8, 9, 10, 11, 12] has been extremely useful in complementing the experimental findings with a more precise characterisation of the folding pathway, albeit obtained for models that greatly simplify the complexity of the real system.

In this paper we propose a theoretical scheme to study the folding of proteins with disulfide bonds by suitably exploiting the (known) protein native structure. At a general level our strategy falls in the class of approaches that build on the importance of the native state topology in steering the folding process[13], that is in bringing into contact pairs of amino-acid that are found in interaction in the native state. In the past few years an increasing number of experimental and theoretical studies have confirmed the utility of these approaches in the characterisation of various aspects of protein folding processes [14, 15, 16, 17, 18, 19, 20, 21, 22, 23, 24, 25, 26]. In the present work we try to generalise this strategy by adding a suitable treatment of disulfide bonds accounting both for their strength as well as their capability to undergo intra-molecular reshuffling.

In order to validate this approach we investigate the folding process of the N-terminal core domain of hirudin HM2 from the blood-sucking leech *Hirudinaria manillensis* [27]. Hirudins are the most potent and specific inhibitors of

thrombin (a key enzyme in blood coagulation) identified so far, and they are currently used as effective anticoagulants. Hirudin HM2 is composed of a compact N-terminal domain (residues 1-47) stabilised by three disulfides (Cys6-Cys14, Cys16-Cys28, Cys22-Cys37) and a highly flexible, negatively charged C-terminal tail. Structural studies conducted on several leech-derived disulfide-rich small proteins (i.e., hirudin, decorsin, and antistasin) reveal that although these proteins display negligible sequence similarity and different function they share a common disulfide topology and 3D fold [28], suggesting that leeches use the same protein scaffold but different binding epitopes to affect hemostasis. Notably, it has been found that these leech antihemostatic proteins possess a T-knot scaffold closely similar to that observed for other unrelated proteins, including b-transforming growth factors, wheat germ agglutinins and snake venom toxins [29, 30]. In this view, the results of our study may have relevant and more general implication on the elucidation of the folding pathway(s) of other protein systems.

The first experimental attempts to identify the folding pathway of Hirudin date back to the studies of Otto and Seckler who argued that Hirudin could be a viable alternative to BPTI and showed that it was experimentally feasible to obtain and follow its unfolding/refolding processes[31]. As for the case of BPTI, also Hirudin has been studied in different experiments [31, 32, 33, 34] leading to alternative formulations of its folding pathway [32, 34]. In particular when dissolved atmospheric oxygen was used as oxidising agent, the folding process appeared to occur first through the establishment of three non-native (scrambled) disulfides and later through their slow rearrangement into the native bonding pattern. On the contrary, no evidence for the importance of these fully-oxidised disordered intermediates was found in the experiments of Thannauser *et al.* carried out using oxidised DL-dithiothreitol (DTT<sup>ox</sup>).

These alternative views prompted the present investigation of the Hirudin pathway within a topology-based model. To ascertain that, despite its simplified nature, the model was suitable to characterize the main aspects of the folding process we have first tuned and validated it against the set of experimental measurements provided in ref. [34]. Based on the success of this comparison we have undertaken a detailed characterisation of the folding process by monitoring quantities inaccessible in previous experiments. Our study confirms the experimental evidence of ref. [34] suggesting that, under a certain set of experimental conditions, the rate-limiting step of the refolding process involves a transition from a species with two disulfides to ones with the three native disulfides[34]. A detailed analysis of the numerical dynamical trajectories further reveals the precise order of formation of the disulfide bonds.

## THEORY AND RESULTS

The starting point of our analysis is the 1-47 fragment of Hirudin[33] resolved by NMR [35] shown in Fig. 1 (see Methods and Materials Section). The fragment under consideration contains three disulfide bonds between residues 6-14, 16-28, 22-37 and differs from the whole protein because it lacks the 18-residues long tail; this tail plays an important role in the biological activity of the protein. However, it is highly mobile due to the virtual absence on any non-covalent contacts with the 1-47 globular fragment. For this reason we neglected the Hirudin tail in our numerical characterisation of the folding process.

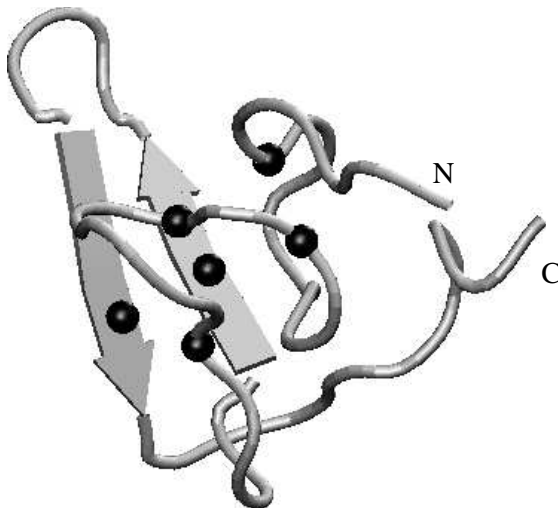


FIG. 1: Native structure of the 1-47 fragment of hirudin. The six cysteine residues, 6, 14, 16, 22, 28, 37 have been highlighted.

The effective energy scoring function that we adopted belongs to the class of topology-based Hamiltonians [13, 36]. The knowledge of the above mentioned native structure,  $\Gamma^N$ , is exploited to construct an effective energy function that admits  $\Gamma^N$  as the lowest energy state. The simplest form of such energy function is as follows:

$$E(\Gamma) = - \sum \Delta_{ij}(\Gamma^N) \cdot \Delta_{ij}(\Gamma) , \quad (1)$$

where  $E(\Gamma)$  is the energy of a trial conformation  $\Gamma$  and  $\Delta(\Gamma)$  is its contact matrix, whose elements are 1 [0] if amino acids  $i$  and  $j$  are [not] in interaction. A standard criterion based on  $C_\alpha$  or  $C_\beta$  distance of pairs of amino acids is used to decide whether two amino acids are interacting.

In the simple case of eqn. (1) the energy minimum is attained when all native bonds are established. Such native interactions are weighted equally. This is a simplification that can be justified when the effective amino acid interactions in the protein are of comparable strength and has the advantage of keeping the model transparent by avoiding the use of imperfect energy parametrisation [37, 38, 39, 40].

It is important to notice that the equal weighting of native contacts does not imply that, in a thermalised ensemble, they are formed with equal probability. In fact, it is the complex interplay of energy and structural entropy that dictates the most probable routes to the native state from an unfolded conformation as well as the presence of rate-limiting steps due to the establishment of crucial sets of native contacts[22].

In the present study, the equal weighting of native contacts does not appear to be a good starting point since one has to account for the very energetic disulfide bridges that can occur between pairs of Cys. For this reason, in place of (1) we adopt a scoring function consisting of two terms (see also section Methods and Materials):

$$\mathcal{H} = V_{n-ss} + \mu V_{ss} . \quad (2)$$

$V_{n-ss}$  enforces some general constraints on the peptide chain geometry and promotes the formation of native contacts between pairs of amino acids other than Cys-Cys. These contacts are weighted in the same manner. The second term,  $V_{ss}$  rewards the formation of disulfide bonds between pairs of cysteines. It is important to stress that the formation of disulfide bonds is allowed among any pair of Cys, not only the native ones. By doing so we can investigate the extent to which species with one or more non-native disulfides are present and if they influence the dynamics toward the native state, as proposed in recent experiments.

The strength of the disulfide bonds relative to other non-covalent interactions is controlled by the parameter  $\mu$ . This parameter should not be regarded as a relative measure of the “bare”, i.e. in vacuum, disulfide strength. In fact, since our model does not treat the solvent explicitly,  $\mu$  captures the effective strength of disulfide bonds in the presence of water and any other appropriate reducing/oxidising agent. For this reason the value of  $\mu$  and also that of the heat bath temperature,  $T$ , have to be chosen in a suitable way so to reproduce as accurately as possible the conditions of a given experiment.

In this study we shall focus on the set of experiments carried out by Thannhauser *et al.* [34] where hirudin was refolded in the presence of various concentrations of  $DTT^{ox}$ . We shall first show that there exists a well-defined region in the  $\mu - T$  parameter space where the rates of conversion between species with different numbers of disulfides match well those observed in experiments. This is an important fact since it proves that, despite its simple form, the energy scoring function of eqn. (2) can indeed be used to characterize the folding process obtaining the correct quantitative experimental picture. Based on such stringent validation of our strategy, we shall then monitor quantities that are inaccessible in current experiments and thus propose a vivid and detailed picture for the hirudin refolding process.

We want to stress the fact that the possibility to reproducing the results of Thannhauser *et al.* [34] for a suitable choice of the  $\mu - T$  parameters support the hypothesis that our model is general enough to study any folding process involving the formation of disulfide bonds.

### Comparison with experimental rates

The experimental benchmark for our model is provided by a series of hirudin refolding experiments carried out by Thannhauser *et al.* [34] under various concentrations of  $DTT^{ox}$ . By using several combined techniques it was established that the refolding process occurs under the reaction shown in Fig. 2 where  $R$ ,  $1S$  and  $2S$  denote respectively the species with 0, 1 and 2 disulfides (either native or non-native). A certain species with three disulfides, denoted as  $3S^*$  was seen to convert with extreme rapidity to native hirudin and was, therefore, identified with a native arrangement of the three disulfide contacts. The remainder of the ensemble of structures with three disulfides (i.e.

with at least two non-native disulfides) is therefore denoted as  $3S$ . The experimental characterisation of Thannhauser *et al* provides the rates for the individual reactions of the above model for a few choices of the initial concentrations of  $DTT^{ox}$  and the reduced protein species. Our first goal was to see if, for suitably chosen values of  $T$  and  $\mu$  it was possible to reproduce such rates.

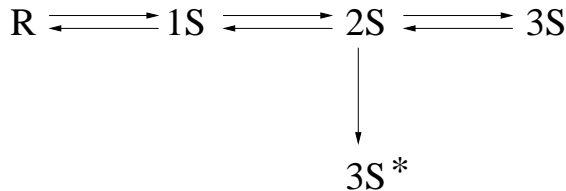


FIG. 2: Best fit model of Thannhauser *et al.* [34] to the hirudin refolding experiments. Species with 0, 1 and 2 disulfides are denoted as  $R$ ,  $1S$  and  $2S$ , respectively. The species denoted as  $3S^*$  contains the three native disulfides. The remainder of the ensemble of structures with three disulfides is therefore denoted as  $3S$ .

Several values of  $T$  and  $\mu$  were considered and, for each of them, we measured the rates of conversion between the  $R$ ,  $1S$ ,  $2S$ ,  $3S$  and  $3S^*$  species by using a Monte Carlo technique. This was done by keeping track of how many transitions out of any given species occurred and how many of them ended up in each of the other species. To ensure that the obtained dynamics could be interpreted as a (coarse grained) viable dynamical trajectory [41] only tiny local distortions of the peptide chain were attempted in the Monte Carlo moves. During such coarse-grained trajectories the formation, breaking or reshuffling of disulfide bonds obeys a set of constraints dictated by the chemistry of the disulfide bonds and the thiol-disulfide coupling. In particular no Cys residue is allowed to participate to more than one disulfide; the number of disulfide bonds can decrease or increase by at most one unit at each time step, respectively when an existing disulfide is broken or through the establishment of a new disulfide between two previously unbonded Cys residues. Intramolecular rearrangements where one bond is broken in favour of a new one (thus preserving the total number of disulfides) are also allowed under the requirement that the new bond involves one of the cysteines of the broken disulfide.

A particular care is necessary to ensure that the Monte Carlo dynamics subject to these constraints does not violate detailed balance. The difficulties arise from the fact that an elementary MC distortion of distinct starting configurations may result in structures that are compatible with a different number of allowed disulfide bonding patterns.

To overcome this problem we have proceeded as follows: to a newly generated conformation  $\Gamma$  we randomly associate one of the 15 possible pairing patterns of the three disulfides. If the proposed bonding pattern of the new structure violates the previous criteria, the structure is rejected and time is incremented. Otherwise, the energy function is recalculated and the structure is rejected or accepted with the usual Metropolis criterion (see Methods for further details). In this way, detailed balance is obviously satisfied, since the same number of bonding patterns is proposed for each structure. The downside is that one encounters frequent Metropolis rejections due to the “blind” proposal of bonding patterns.

For each of the explored values of  $T$  and  $\mu$  we have measured the correlation between the experimental rates and those obtained numerically. As a measure of the degree of correlation between these two quantities we used the non-parametric Kendall analysis [42]. This statistical tool allows to establish if there is a relationship between two sets of data and how statistically significant it is. Being based on the comparative ranking of corresponding data in the two sets, the Kendall analysis does not rely on any pre-assigned parametric dependence (e.g. linear) between the two quantities. For this reason, it is regarded as a very robust measure of correlation and appears particularly appropriate in this context where the measured rates (both experimental and numerical) span several orders of magnitude [42].

Our findings are summarised in Fig. 3 where we have shown the contour and density plot of the Kendall correlation coefficient,  $\tau$ , against the rates pertaining to the experimental conditions of Fig. 5a in ref. [34]. These effective first-order like rates were obtained starting from the best-fit experimental rates of Table 2 in ref [34] multiplied by the asymptotic concentration of  $DTT^{ox}$  or  $DTT^{red}$  measured under the given experimental conditions (see Fig. 6 in the same reference). A darker/lighter shadow in Fig. 3 denotes the presence of a higher/lower degree of correlation. It is apparent that the experimental data are well reproduced in the neighbourhood of  $\mu = 2.8$ ,  $T = 1.0$  for which the highest correlation  $\tau = 0.81$  is observed. To ascertain the statistical significance of observing such correlation, we have computed the probability to observe, by pure chance a correlation larger than the observed one. It turns out that this probability (double-sided) is equal to  $p = 0.01$ , which testifies the statistical significance of the observed correlation. This establishes that there is a strong monotonic relation between the experimental and theoretical rates.

A scatter plot of the logarithm of experimental rates versus the numerically obtained ones is provided in Fig. 4

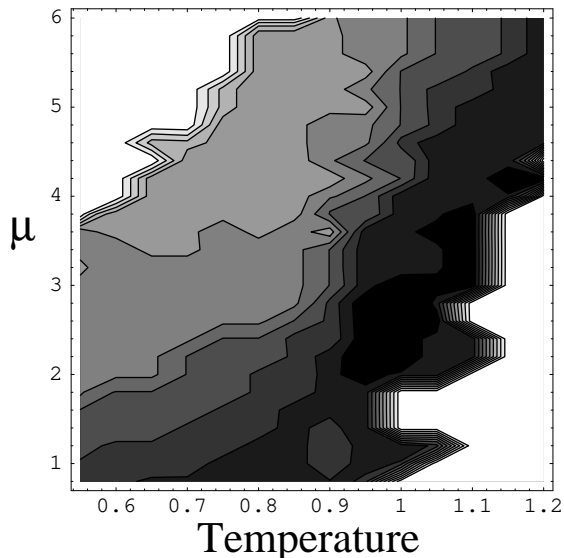


FIG. 3: Contour and density plot of the Kendall correlation across the  $T - \mu$  plane. The white regions correspond to the minimum values of the correlations were observed ( $\tau \approx 0$ ). The highest correlation,  $\tau = 0.81$ , was observed in the dark area located around  $\mu = 2.8$ ,  $T = 1.0$ .

where the good interdependence of the data can be visually inspected. If one were able to model the folding process with detailed and accurate energy functions one would expect an equality of the theoretical and experimental rates, a part from a time conversion factor. In our case, due to the simplicity of our model we do not observe such dependence but encounter, instead, another simple linear relationship between the logarithms of both sets of rates. This is visible in the linear fit of Figure 3; the corresponding correlation coefficient is  $r = 0.88$ . Its statistical significance (two-sided) over the set of 7 data points is 4% which is compatible with the significance of the more general (and robust) Kendall correlation. These values indicate that the correlation is highly significant from the statistical point of view.

A further validation can be carried out by comparing the asymptotic concentration of the various species observed in the experiment and in an equilibrated MC trajectory. In case of a perfect correlation between the experimental and numerical rates, this further check would be redundant. In this context, where the correlation is not perfect (a significant discrepancy is seen for the transition between the  $3S$  and  $2S$  species) this validation is useful to ascertain whether the differences in the rates result in significantly different equilibrium conditions. The plot of Fig. 4b reveals that the asymptotic concentrations are in good accord and hence by setting  $T = 1$  and  $\mu = 2.8$  one can be confident that the MC trajectory is compatible both the dynamical and equilibrium properties of the experimental system.

### Thermodynamics

It is interesting to analyse the thermodynamic behaviour of the system at  $\mu = 2.8$  as a function of the heat bath temperature,  $T$ . By using the standard, yet powerful method of histogram re-weighting (see Methods) we have computed the average internal energy as a function of  $T$ . The data, shown in Fig. 5(a) indicate the presence of a point of inflection for temperatures close to 1. The presence of a transition at this temperature is further corroborated by the behaviour of the specific heat  $C_v$  which displays a clear peak at  $T = T_F \approx 0.91$ , the folding temperature, and by the presence of two minima in the free energy profile in Fig. 5(b).

This peak is associated to the folding transition in the system and its neatness suggests that the folding process has a two-state character [12]. This is indeed confirmed by an analysis of the free energy landscape at  $T_F$  which exhibits two minima as a function of  $V_{n-ss}$  in correspondence of the unfolded and folded states (data not shown). The special point  $\mu = 2.8$ ,  $T = 1.0$ , corresponding to the experimental conditions of ref. [34] appears therefore to be

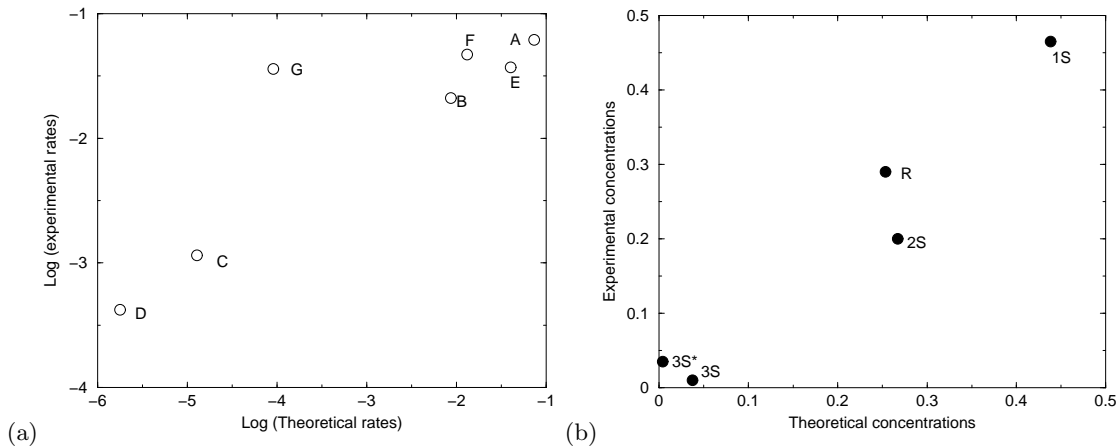


FIG. 4: (a) Linear correlation between the log of experimental rates of Figs. 5a ref. [34] and those obtained through the present numerical calculation for  $\mu = 2.8$ ,  $T = 1.0$ . The experimental rates are expressed in  $\text{min}^{-1}$ . The points in the plot correspond to the following transitions A:  $R \rightarrow 1S$ , B:  $1S \rightarrow 2S$ , C:  $2S \rightarrow 3S$ , D:  $2S \rightarrow 3S^*$ , E:  $1S \rightarrow R$ , F:  $2S \rightarrow 1S$ , G:  $3S \rightarrow 2S$ . (b) Scatter plot of the equilibrium fraction of the various species obtained in the Monte Carlo trajectory and in the experiment. The experimental concentrations were extracted from Fig. 5a of ref[34] for  $t = 500$  s.

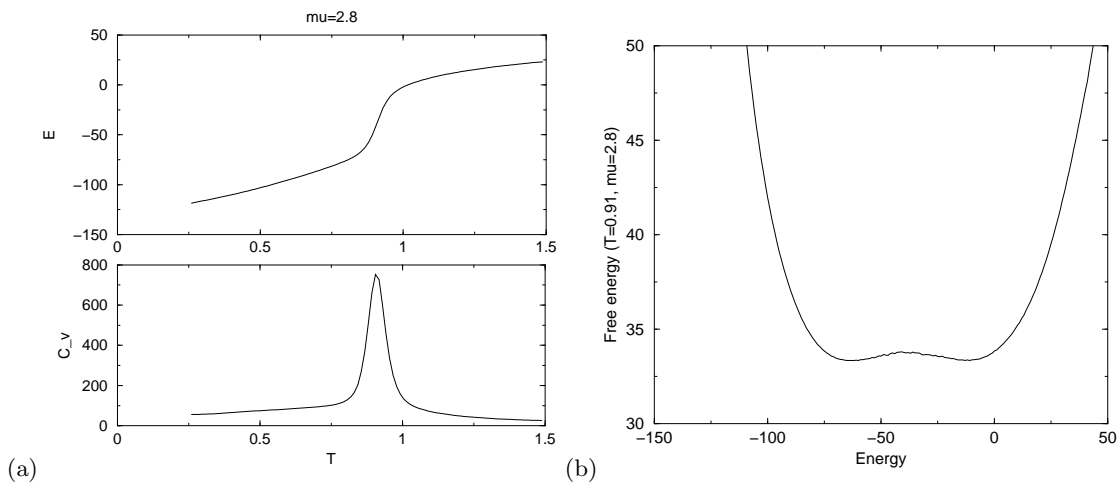


FIG. 5: (a) Total energy and specific heat for  $\mu = 2.8$ . (b) Free energy profile, as a function of the internal energy, at the point  $\mu = 2.8$ ,  $T = 0.91$ .

located slightly above the folding transition temperature (for  $\mu = 2.8$ ). This is entirely consistent with the fact that the experimental conditions of ref. [34], Fig. 5a, do not particularly favour the formation of the native state which, indeed, involves only a few percent of the total equilibrium population.

We have portrayed in Fig. 6 the free energy landscape for the different reduced species as a function of  $V_{n-ss}$ . It can be seen that the free energy profiles have minima at different energy values according to the number of correctly formed disulfides. The  $R$ ,  $1S$ ,  $2S$  and  $3S$  species, in fact, display a minimum near  $E \approx 0$  which denotes an unfolded ensemble (see Fig. 5b). On the contrary, the species with three native disulfides has a free-energy minimum for energies much closer to the native state energy.

The relative high values of free energy associated to the  $3S^*$  species reflect the particular experimental conditions reproduced here where the asymptotic fraction of species with native disulfides is low. Clearly, by lowering the temperature one favours the formation of the native structure which is accompanied by an increase of the concentration with native bonding patterns for the cysteines. This effect is visible in Fig. 7a where the average fraction of formed disulfide bonds is portrayed as a function of temperature. It can be seen that above  $T_F$  one has a significant formation of non-native bonds, that are superseded by native ones below  $T_F$ .

An alternative picture to this one was put forward by Chatrenet and Chang based on a hirudin refolding experiment carried out in ref. [32]. Due to the much more oxidising conditions than the one considered in ref. [34], Chatrenet and

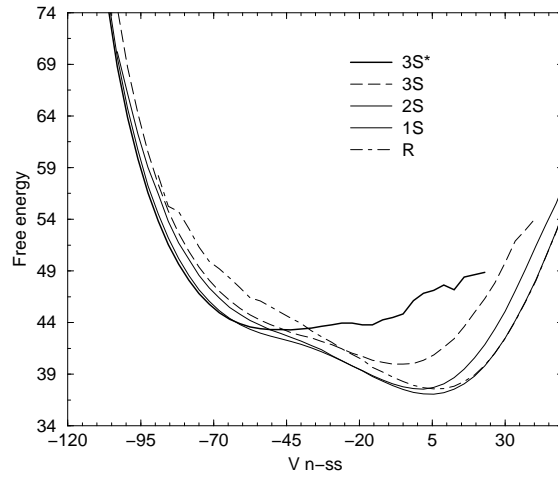


FIG. 6: Free energy profile for  $T = 1.0$  and  $\mu = 2.8$  of the  $R$ ,  $1S$ ,  $2S$ ,  $3S$  and  $3S^*$  ensembles as a function of  $V_{n-ss}^N$ .

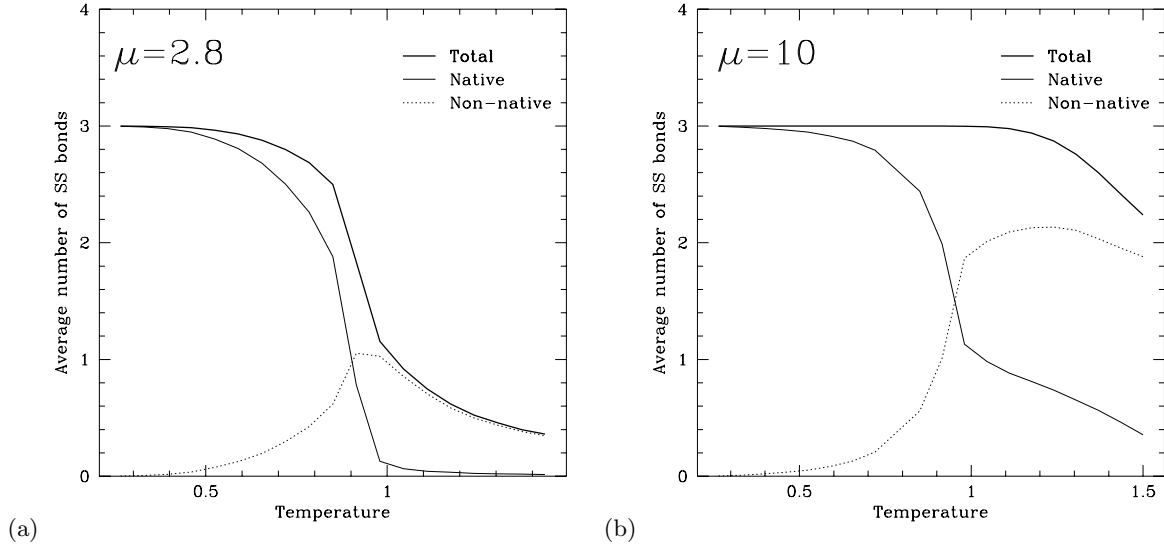


FIG. 7: Average number of total (thick continuous line), native (continuous line) and non-native (dotted line) disulfide bonds for (a)  $\mu = 2.8$  and (b)  $\mu = 10$ .

Chang [32] observed that the folding of hirudin occurred through the formation of intermediates with three (typically non-native) formed disulfides. Through a slow reshuffling process the disulfides would then rearrange in the native pairing from which the native conformation could be easily reached.

Our findings indicate that this alternative scenario could be probably captured by our model by using larger values of the effective disulfide strength  $\mu$ . This is consistent with the different oxidising solvent conditions [34] adopted by Chatrenet and Chang.

To investigate this regime we explored the value of  $\mu = 10$ . It is important to point out that the folding transition temperature (identified through the location of the specific heat peak) is almost insensitive to the disulfide strength in the range  $0 \leq \mu \leq 10$ . By comparing the plots in Fig. 7 it is then possible to see that for the higher value of  $\mu$  the total number of formed disulfide bonds is higher than for  $\mu = 2.8$ . This result, accompanied by the fact that the total energy depends weakly on  $\mu$ , confirms the intuition that, for large  $\mu$ 's the disulfides are established at early stages of the folding process when the rest of the protein is still unstructured. This “greedy” disulfide formation not only impacts on the total number of formed disulfides but also on the relative fraction of correct (native ones). As a result, a much higher fraction of wrong bonds is found at any temperature, as noticeable in Fig. 7b. This picture suggests that the large  $\mu$  regime of our model may be compatible with the scenario proposed by Chatrenet and Chang where

the rate-limiting step corresponded to the disentanglement of non-native disulfides in intermediates states with three formed disulfide bonds. However, for this alternative case the experimental rates are not available and we cannot corroborate in a more quantitative way the parallel between the experimental conditions of Chatrenet and Chang and the “large”  $\mu$  regime in our model.

### FOLDING PATHWAYS

So far we have focused on the overall thermodynamic characterisation of the refolding of hirudin, paying a particular attention to the validation of our model against experimental data. Having established that the detailed experimental reaction rates of ref. [34] can be well reproduced we can confidently use our model to investigate finer aspects of the refolding process.

We begin by examining the details of formation of the native arrangement of disulfides. Our interest is to find whether the formation of the  $3S^*$  species is aided by the establishment of some non-native disulfides that are later broken in favour of native bondings. To do so, instead of subdividing the structures according to just the overall number of disulfides we indexed them with a pair of numbers,  $(n_c, n_w)$  denoting the number of correct (native) disulfides,  $n_c$  and wrong (non-native) ones,  $n_w$ . In this way the fully reduced state,  $R$ , is indicated as  $(0,0)$  while the  $3S^*$  state corresponds to  $(3,0)$ . Altogether there are nine possible states, as indicated in Fig.8.

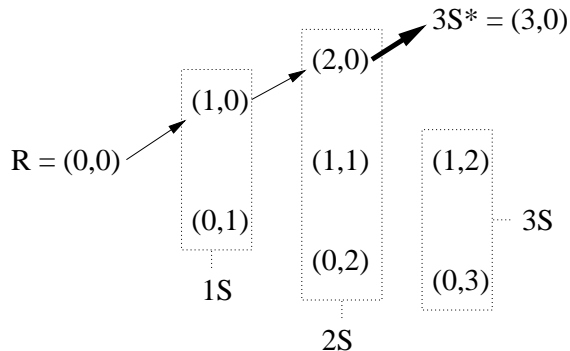


FIG. 8: The different states considered in our trajectory analysis. The arrows indicate the most probable route from the reduced ensemble toward the native arrangement of disulfides. The thickest arrow denotes the rate-limiting step of the reaction.

We have generated several MC trajectories, each spanning about 20 million time steps (see sections Methods and Materials) at  $(T = 1.0, \mu = 2.8)$  and then recorded the probability of occurrence of all allowed transitions between the states of Fig. 8. The typical dispersion on the measured rates over ten MC trajectories was typically less than 1% but augmented to about 10 % for the few very improbable transitions. Then we have considered all possible productive routes taking from  $R$  to  $3S^*$  in a preassigned number of transitions. The probability of occurrence for any such routes is obtained by multiplying the individual probabilities of any of the elementary steps. By considering productive routes involving an increasing number of transitions it can be established that the most probable route (see Fig. 8) is  $R \equiv (0,0) \rightarrow (1,0) \rightarrow (2,0) \rightarrow (3,0) \equiv 3S^*$  which is more than ten times as likely than the second ranking paths which is  $R \rightarrow (0,1) \rightarrow (1,0) \rightarrow (2,0) \rightarrow 3S^*$ . These findings seem robust against variations of the parameters in our model. For example, even changing the temperature to 0.8 (keeping  $\mu = 2.8$ ) so that the formation of native species is strongly favoured (see Fig. 7a) it is found that the top ranking routes taking from the reduced state to the native one are the same as above. Interestingly, the relative weight ratio of the top productive routes is analogous to the one encountered for  $T = 1.0$ ; on the other hand the fact that the native formation is highly favoured at  $T = 0.8$  is reflected in an increase, by several orders of magnitude, of the weight of the productive routes.

We complete the present section by identifying the rate limiting steps of the folding process. In a sequential reaction the rate limiting step is straightforwardly identified as the slowest one. In the present scheme such simple analysis cannot be carried out due to the presence of several alternative routes that can take to the native state. An objective and convenient way to identify the rate limiting step in such a situation is to identify the reaction whose rate change affects the most the production of the species of interest, in this case  $3S^*$ . Therefore, by using the measured rates for the transitions between the states of Fig. 8 we have integrated the associated master equations starting from a fully reduced population. We have then changed by 10 % each of the rates and identified the time at which the concentration of  $3S^*$  crosses a pre-assigned threshold value. We found that, almost independently of the threshold



value, the most sensitive step among all the allowed ones was  $(2, 0) \rightarrow 3S^*$  which is the last step of the most probable route leading to  $3S^*$ . In principle this may have not been the case, especially in the presence of equally important paths leading to  $3S^*$ . The fact that the most probable routes include the rate limiting steps confirms the existence of a well defined succession of events taking to the native state.

As mentioned before, based on experimental dynamical plots, Thannhauser *et al.* [34] had determined that the rate limiting step was the  $2S \rightarrow 3S^*$  one. In their study it was not possible to characterise by direct means whether the transition to the  $3S^*$  state occurred from a  $2S$  state comprising only native cysteine bonds, although this was reputed to be the most likely scenario. Our picture thus fully supports the experimental results concerning the  $2S \rightarrow 3S^*$  rate-limiting step, but also adds novel insight in the process by indicating explicitly that the most crucial step involves a particular  $2S$  species, namely one with two native disulfides. In the remainder of this section we shall further characterise the folding process by identifying which of the native disulfides are formed in the most probable routes (or rate-limiting steps). This is done by following a series of individual dynamical trajectories where the native conformation is reached starting from a reduced state.

### Folding trajectories

The Monte-Carlo procedure allows for a detailed study of the folding pathways and for a systematic analysis of the specific order of formation of disulfide bonds. By setting  $\mu = 2.8$  the protein is initially thermalised at a high temperature ( $T \sim 10$ ) where, in our model, the disulfide bonds are completely reduced and then suddenly quenched to  $T = 1.0$ . For each kinetic trajectory the order of formation of the disulfide bonds was stored and a statistical analysis accomplished by comparing several runs. In particular we have recorded the exact type of disulfide bridges forming the different species ( $1S, 2S$ ) and from their relative concentration we have inferred the pathway.

The six Cys residues of the fully reduced protein, 6, 14, 16, 22, 28, 37 are equally likely to participate in forming the initial disulfide bond. Although in the early folding stages the contact (14 – 16) appears quite frequently due to the short sequence distance between the amino-acids, after the molecule has equilibrated through a series of rapid internal disulfide interchange reactions, only 5 of the 15 possible  $1S$  states exist in significant quantities. They are: (6-14), (6-16), (16-22), (28-37) that are respectively present in the following equilibrium concentrations: 7% 6% 12% and 26%. It is interesting to notice that the most common bond among the  $1S$  ensemble is a non-native one, (28-37), while the only native bond that is present in significant quantities is (6-14).

Of the 45 possible  $2S$  states, seven occur in significant quantities. Two of them, (6-14;16-28) present in the 1% of the cases and (6-14,22-37) present in the 0.7% of the cases, are formed by native bonds. Other two, (6-14;16-22) and (6-14,28-37) present with concentration of 2% and 5% respectively, have a native and a non-native contact. Whereas the last three, (6-16,28-37) with a frequency of 9%, (14-22,28-37) with a frequency of 7% and (16-22,28-37) with a frequency of 7%, are formed by non-native disulfide bonds. The relatively high concentration of species with non-native states, which are not present in the most probable productive routes expected for the folding (see the previous section), reflect the particular experimental conditions reproduced here (induced by the choice of  $T$  and  $\mu$ ) in which the formation of the native state is not particularly favoured (see Fig. 4b).

The analysis of the folding pathway reported in the previous section and the statistical analysis of the dynamical productive pathway can be summarised in the following re-folding picture: the reduced proteins forms first the native contact (6 – 14) and consequently either the states (6-14;16-28) or (6-14,28-37) almost with the same probability. The folding proceeds with the formation of the last disulfide bond. This conversion is relatively slow in agreement with the finding of the previous section on the rate limiting step of the reaction. The presence of conformation with three scrambled disulfide bonds turns out not to be statistically significant also from this kinetic analysis. A graphical representation of the most probable trajectory is shown in Fig. 9.

The fact that the majority of structures sampled in the quenching process involve non-native bonding patterns is not in contradiction with the findings of the previous section, where the most probable *productive* route was shown to be free of non-native bonds. In fact, the high concentration of structures with non-native bonds does not automatically imply that they contribute significantly to the refolding “flux” towards the native state. On the contrary, species involving native bonds even if they do not accumulate to high equilibrium concentration, appear to take part to the most efficient routes leading to the native state.

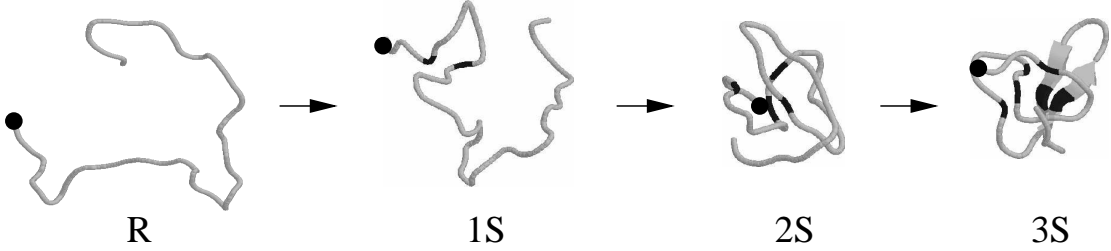


FIG. 9: Snapshots of one of the possible folding trajectories. The 1S state involves the native contact (6-14), while the 2S species involves the native bonds (6-14) and (16-28). A black sphere is used to distinguish the N-terminus while cysteines involved in disulfide bonds are highlighted as dark segments.

## METHODS AND MATERIALS

### Structure of Hirudin

The structure of the synthetic analogues of fragment 1-47 of hirudin HM2 in the free state was modelled on the NMR solution structure of natural fragment 1-47 [35], almost super-imposable to that of the corresponding segment (1-49) in intact hirudin HV1 variant[43] (PDB code: 5HIR), showing 75% sequence identity with hirudin HM2, or to that of HV1 fragment 1-51 [44] (PDB code: 1HIC). The best-representative model in the NMR ensemble was selected using the program OLDERADO [45] available on-line at the site <http://neon.chem.le.ac.uk>.

### The Model

In our model a generic conformation  $\Gamma\{\vec{r}_i\}$  of the protein is modelled as a self-avoiding chain of connected  $C_\alpha$  atoms located at position  $\vec{r}_i^\alpha$ , where  $i$  is the amino-acid chain index (ranging from 1 to 47). Starting from the  $C_\alpha$  coordinates the peptide dihedral angles are calculated and hence, following standard geometrical rules [39, 46] we construct an effective  $C_\beta$  centroid for all residues with the exception of the two end residues and the seven Glycines (indices: 10,18,23,25,34,40,42).

The energy scoring function consists of two terms. The first one incorporates a standard bias toward the formation of native non-disulfide bonds but also disfavours the formation of non-native bonds (except for disulfide ones) and penalises significant deviations from the native dihedral angles. These details are known to improve the cooperatively of the modelled folding process [47, 48, 49, 50]. The explicit expression of this term, evaluate on a trial structure  $\Gamma$  is given by:

$$\begin{aligned}
 V_{n-ss}(\Gamma) = & \\
 & V_0 \sum'_{i,j>i+2} \Delta_{ij}(\Gamma^N) \left[ 5 \left( \frac{r_{ij}^N}{r_{ij}} \right)^{12} \right. \\
 & \quad \left. - 6 \left( \frac{r_{ij}^N}{r_{ij}} \right)^{10} \right] \\
 & + V_1 \sum'_{i,j>i+2} [1 - \Delta_{ij}(\Gamma^N)] \left( \frac{r_{ij}^N}{r_{ij}} \right)^{12} \\
 & + V_2 \left[ \sum_{i=2,46} (\theta_i - \theta_i^N)^2 + \sum_{i=3,46} (\phi_i - \phi_i^N)^2 \right] \\
 & + V_{constraints}
 \end{aligned} \tag{3}$$

$$\tag{4}$$

where  $r_{ij}$  denotes the distance of the  $i$ th and  $j$ th  $C_\alpha$  atoms in the trial structure  $\Gamma$ ; a superscript  $N$  is used to denote analogous quantities pertaining to the native structure. The contact map  $\Delta$  is computed by considering as threshold a distance of 8 Å between the  $C_\alpha$  atoms. The prime in the summation indicates that no contribution is considered if both the amino-acids are Cys. Finally, the angular term has been constructed using the standard dihedral angles,

$\theta$  and  $\phi$  [39, 46]. The coefficients  $V_0, V_1$  and  $V_2$  are used to control the strength of interactions and are set equal to 1, 5 and 1 energy units, respectively. The last term in the expression,  $V_{constraints}$ , is used to enforce a series of knowledge-based constraints whose violation is penalised through an “infinite” energy penalty (that is through a rejection of the violating conformation). The constraints are as follows: (1) the distance between two consecutive  $C_\alpha$  atoms must remain in the interval 3.7-3.9 Å, (2) the distance between two non consecutive  $C_\alpha$  atoms must be greater than 4 Å, (3) the distance between any two  $C_\beta$  must be greater than 2 Å and (4) the distance between any two  $C_\alpha$  and  $C_\beta$  centroids must be greater than 2 Å.

The second term of the Hamiltonian,  $V_{ss}$  rewards the formation of disulfides, irrespective of whether they are native or not. As explained in the next subsection, each proposed configuration, described in terms of  $C_\alpha$ ’s and  $C_\beta$ ’s, comes with a set of three putative bonds among the six cysteines. Of these putative bonds only those among residues whose  $C_\beta$ ’s are a separation smaller than 5 Å are considered to be effectively present and hence give a contribution equal to  $-\mu$  to the total energy.

### Monte-Carlo Method

As mentioned in the text, we used Monte Carlo dynamics for studying the folding process. At each Monte-Carlo step the current structure is distorted through local deformations [51] based on two equally-probable moves: (a) *single-bead move*: a random *alpha*-carbon is chosen and is displaced randomly by at most 1 Å along each Cartesian direction, (b) *crankshaft move*: two sites,  $i$  and  $j$ , with sequence separation at most 6 are chosen and all the sites between them are rotated around the axis joining  $i$  and  $j$  by an angle chosen randomly in the interval  $-\frac{\pi}{10} \leq \Omega \leq \frac{\pi}{10}$ . As mentioned before, besides this structural rearrangement, at each Monte Carlo step we also associate a randomly-chosen pairing pattern for the six cysteines so that each of them is involved in a *putative* disulfide bond. These bonds are termed putative because, to satisfy detailed balance, the pairing assignment is done blindly that is without inspecting whether a given pair of cysteines is at a distance compatible with the existence of a disulfide bond. One then checks whether (irrespective of the pairing distances) the proposed bonding pattern is compatible with the undistorted configuration, i.e. if it respects the rules of section 2.1 about disulfide formation and thiol/disulfide coupling. If not the configuration is rejected, the Monte Carlo clock is advanced and a new distortion and bonding pattern is considered. Otherwise one proceeds as in ordinary Metropolis schemes after having calculated the energy of the proposed configuration. It is important to notice that this latter step involves the inspection of the distance of the putatively bonded cysteines to reward only those bonds that are geometrically feasible.

The efficiency of the Monte-Carlo algorithm to study the thermodynamics was enhanced by the multiple Markov-chain sampling scheme[52], a method that has proved quite effective in exploring the low temperature phase diagrams of proteins and interacting polymers. All the runs have been performed by covering the temperature range of interest,  $T = [0.2, 1.5]$ , with 20 Markov chains uniformly-spaced in temperature.

The data obtained in the multiple-Markov-chain runs at different values of  $T$  and  $\mu$  were further processed through a generalised multiple histogram technique inspired by the work of ref. [53]. This strategy allowed to reconstruct faithfully the density of states (number of configurations) in the multi-dimensional space of reaction coordinates constituted by  $V_{n-ss}$  and the number of correct (native) and wrong (non-native) disulfides:  $(n_c, n_w)$ . The data from the different runs were combined so to minimize the error propagation on the density of states. The typical uncertainty of the reconstructed free-energy at the values of  $T$  and  $\mu$  considered here is about 0.5 energy unit (this estimate follows from the analysis of free energy dispersion when half of the collected data is used). By these means it was possible to obtain the total energy and specific heat curves of Fig. 5 and the free energy profiles of Fig. 6.

### CONCLUSIONS

We have proposed a theoretical framework to model and study the folding of proteins containing disulfide bonds. The approach is based on the knowledge of the native state of a protein but contains an appropriate term to account for the possibility that native or non-native disulfide bonds can form. The main advantage of the model proposed here is its simplicity which allows for a detailed description of all the folding pathways through the monitoring of the correct/incorrect contact formation.

The model has been validated by investigating the debated re-folding pathways of Hirudin which has been object of several experimental studies. It was shown that there exists a region in our two-dimensional parameter space where the rates of conversions between different oxidised species are in good agreement with experimental measurements

[34]. Starting from this successful comparison we have then attempted a detailed characterisation of the whole folding process.

At a coarse-grained level our results is consistent with the scenario described by Thannhauser *et al.* [34] suggesting that the rate limiting step turns out to be  $2S \rightarrow 3S^*$ . Our approach, that allow for a precise identification of the formed contacts, shows clearly that the  $2S$  state appears to involve native intermediates, possibility that was reputed as the most probable situation in ref. [34] although experimentally it was impossible to show it directly. The analysis of several folding trajectories also allowed the identification of the most probable folding route and the typical associated succession of formation of disulfide bridges. Furthermore, the thermodynamics of the system was elucidated by using statistical mechanical techniques to reconstruct the free energy profiles for the whole system and also for the different oxidised species.

Due to its simplicity, the proposed model, cannot capture those aspects of the folding process that result from the delicate interplay of amino acid specific interactions. The successful comparison of the theoretical predictions for hirudin with the experimental findings suggests that also, for disulfide containing proteins, suitable topology-based models can be profitably used to elucidate the folding pathways, even in the presence of non-native intermediates. Thus, the present approach, which is general and not specifically tailored for hirudin, ought to be straightforwardly applicable in other contexts providing a useful complement of experimental techniques in the characterisation of the folding process in the presence of disulfide bonds.

### ACKNOWLEDGEMENTS

We thank F. Cecconi, G.L. Lattanzi and D. Marenduzzo for stimulating discussions and suggestions. This work was supported by INFN, FISR-MIUR 2001 and Murst Cofin 2001.

- 
- [1] Anfinsen, C. Principles that govern the folding of protein chains. *Science* 181:223–230, 1973.
  - [2] Creighton, T. *Proteins, structure and molecular properties*. W.H.Freeman and Company, New York, second edition, , 1993.
  - [3] Creighton, T. The disulfide folding pathway of bpti. *Science* 256:111–114, 1992.
  - [4] Weismann, J. and Kim, P. Reexamination of the folding of bpti: Predominance of native intermediates. *Science* 253:1386–1393, 1991.
  - [5] Creighton, T. The two-disulphide intermediates and the folding pathway of reduced pancreatic trypsin inhibitor. *JMB* 95:168, 1975.
  - [6] Weismann, J. and Kim, P. Kinetic role of nonnative species in the folding of bovine pancreatic trypsin inhibitor. *PNAS* 89:9900–9904, 1992.
  - [7] Scheraga, H., Konishi, Y., Rothwarf, D., and Mui, P. Toward an understanding of the folding of ribonuclease a. *PNAS* 84:5740–5744, 1987.
  - [8] Camacho, C. and Thirumalai, D. Modelling the role of disulfide bonds in protein folding: Entropic barriers and pathways. *PROT* 22:27–40, 1995.
  - [9] Camacho, C. and Thirumalai, D. Theoretical predictions of folding pathways using the proximity rule with application to btpi. *PNAS* 92:1277–1281, 1995.
  - [10] Abkevich, V. and Shakhnovich, E. What can disulphide bond tell us about protein energetics, function and folding:simulations and bioinformatics analysis. *JMB* 300:975–985, 2000.
  - [11] Thirumalai, D., Klimov, D., and Dima, R. Insights into specific problems in protein folding using simple concepts. *Advances in Chemical Physics* 120:35–77, 2002.
  - [12] Chan, H., Kaya, H., and Shimizu, S. in *Current topics in computational molecular biology*, pp. 403-447,. Mit press, Cambridge, USA, , 2002.
  - [13] Go, N. and Scheraga, H. A. On the use of classical statistical mechanics in the treatment of polymer chain conformations. *Macromolecules* 9:535–542, 1976.
  - [14] Micheletti, C., Banavar, J. R., Maritan, A., and Seno, F. Protein structures and optimal folding from a geometrical variational principle. *Phys. Rev. Lett.* 82:3372–3375, 1999.
  - [15] Munoz, V. and Eaton, W. A simple model for calculating the kinetics of protein folding from three-dimensional structures. *PNAS* 96:11305–11310, 1999.
  - [16] Alm, E. and Baker, D. Prediction of protein-folding mechanisms from free-energy landscapes derived from native structures. *PNAS* 96:11305–11310, 1999.
  - [17] Galzitskaya, O. and Finkelstein, A. A theoretical search for folding/unfolding nuclei in three-dimensional protein structures. *PNAS* 96:11299–11304, 1999.

- [18] Maritan, A., Micheletti, C., and Banavar, J. R. Role of secondary motifs in fast folding polymers: a dynamical variational principle. *Phys. Rev. Lett.* 84:3009–3012, 2000.
- [19] Baker, D. A surprising simplicity to protein folding. *Nature* 405:39–42, 2000.
- [20] Clementi, C., Nymeyer, H., and Onuchic, J. Topological and energetic factors: What determines the structural details of the transition state ensemble and en-route intermediates for protein folding? an investigation for small globular proteins. *JMB* 298:937–953, 2000.
- [21] Orlandini, E., Seno, F., Banavar, J., Laio, A., and Maritan, A. Deciphering the folding kinetics of transmembrane helical proteins. *PNAS* 97:14229–14234, 2000.
- [22] Cecconi, F., Micheletti, C., Carloni, P., and Maritan, A. Molecular dynamics studies of HIV-1 protease: Drug resistance and folding pathways. *Proteins: Structure Function and Genetics* 43:365–372, 2001.
- [23] Hoang, T. X. and Cieplak, M. Sequencing of folding events in go-type proteins. *J. Chem. Phys.* 113:8319–8328, 2000.
- [24] Zhou, Y. Q. and Karplus, M. Interpreting the folding kinetics of helical proteins. *Nature* 401:400–403, 1999.
- [25] Shea, J., Nochomovitz, Y. D., Guo, Z., and III, C. L. B. Exploring the space of protein folding hamiltonians: the balance of forces in a minimalist beta-barrel model. *J. Chem. Phys* 109:2895–2903, 1998.
- [26] Plotkin, S. Speeding protein folding beyond the go model: How a little frustration sometimes helps. *PROT* 45:337–345, 2001.
- [27] Scaccheri, E., Nitti, G., Valsasina, B., Orsini, G., Visco, C., Ferreira, M., Sawyer, R. T., and Sarmientos, P. *Eur. J. Biochem.* 214:295–304, 1993.
- [28] Wagner, G., Seymour-Ulmer, J., and Lazarus, R. A. *Science* 264:1944–1947, 1994.
- [29] Lin, S. and Nussinov, R. *Nature Struct. Biol.* 2:835–837, 1995.
- [30] Ascenzi, P., Bolognesi, M., Catalucci, D., Pascarella, S., Ruoppolo, M., and Rizzi, M. *Biol. Chem.* 379:1387–1389, 1998.
- [31] Otto, A. and Seckler, R. Characterization, stability and refolding of recombinant hirudin. *Eur. J. Biochem* 202:67–73, 1991.
- [32] Chatrenet, B. and Chang, J. The disulfide folding pathway of hirudin elucidated by stop/go folding experiments. *Journal of Biological Chemistry* 268:20988–20996, 1993.
- [33] Filippis, V. D., Vindigni, A., Altichieri, L., and Fontana, A. Core domain of hirudin from the leech *hirudinaria manillensis*: Chemical synthesis, purification and characterization of a trp<sup>3</sup> analog of fragment 1-47. *Biochemistry* 34:9552–9564, 1995.
- [34] Thannhauser, T., Rothwarf, D., and Scheraga, H. Kinetic studies of the regeneration of recombinant hirudin variant 1 with oxidized and reduced dithiothreitol. *Biochemistry* 36:2154–2165, 1997.
- [35] Nicastro, G., Baumer, L., Bolis, G., and Tato, M. Nmr solution structure of a novel hirudin variant hm2, n-terminal 1-47 and n64 → v+g mutant. *Biopolymers* 41:731–749, 1997.
- [36] Go, N. and Abe, H. Non interacting local structures. model of folding and unfolding transition in globular protein. i. formalism. *Biopolymers* 20:991, 1981.
- [37] Maiorov, V. N. and Crippen, G. M. Contact potential that recognizes the correct folding of globular proteins. *J. Mol. Biol.* 227:876–888, 1992.
- [38] Thomas, P. D. and Dill, K. A. An iterative method for extracting energy-like quantities from protein structures. *Proc. Natl. Acad. Sci. USA* 93:11628–11633, 1996.
- [39] Micheletti, C., Seno, F., Banavar, J. R., and Maritan, A. Learning effective amino acid interactions through iterative stochastic techniques. *Proteins: Structure Function and Genetics* 42:422–431, 2001.
- [40] Chang, I., Cieplak, M., Dima, R., Banavar, J., and Maritan, A. Protein threading by learning. *Proc. Natl. Acad. Sci. (USA)* 98:14350–14355, 2001.
- [41] Sokal, A. D. Monte carlo methods for the self-avoiding walk. *Nuclear Physics B* 47:172–179, 1996.
- [42] Press, W. H., Teukolsky, S. A., Vetterling, W. T., and Flannery, B. P. *Numerical Recipes*. CUP, Cambridge, , 1999.
- [43] Folkers, P., Clore, G., Driscoll, P., Dodt, J., Koheler, S., and Gronenborn, A. Solution structure of recombinant hirudin and the lys -z; gln mutant: A nuclear magnetic resonance and hybrid distance geometry - dynamical simulated annealing study. *Biochemistry* 28:2601–2617, 1989.
- [44] Szyperki, T., Guntert, P., and et al., S. S. Impact of protein protein contacts on the conformation of thrombin-bound hirudin studied by comparison with the thrombin-bound hirudin studied by comparison with the nuclear magnetic resonance solution structure of hirudin(1-51). *JMB* 228:1206–1211, 1992.
- [45] Kelley, L. and Sutcliffe, M. Olderado: On-line database of ensemble representatives and domains. *Protein Science* 12:2628–2630, 1997.
- [46] Park, B. and Levitt, M. Energy functions that discriminate x-ray and near-native folds from well-constructed decoys. *J. Mol. Biol.* 258:367–392, 1996.
- [47] Chan, H. S. and Dill, K. A. The effects of internal constraints on the configurations of chain molecules. *J. Chem. Phys.* 92:3118–3135, 1990.
- [48] Kaya, H. and Chan, H. S. Energetic components of cooperative protein folding. *Phys. Rev. Lett.* 85:4823–4826, 2000.
- [49] Kaya, H. and Chan, H. S. Polymer principles of protein calorimetric two-state cooperativity. *Proteins: Structure Function and Genetics* 40:637–661, 2000.
- [50] Settanni, G., Cattaneo, A., and Maritan, A. Role of native-state topology in the stabilization of intracellular antibodies. *Biophys. J.* 81:2935–2945, 2001.
- [51] Micheletti, C., Seno, F., and Maritan, A. Recurrent oligomers in proteins - an optimal scheme reconciling accurate and concise backbone representations in automated folding and design studies. *Proteins: Structure Function and Genetics* 40:662–674, 2000.
- [52] Tesi, M., van Rensburg, E. J., Orlandini, E., and Whittington, S. Monte-carlo study of the interacting self-avoiding walk

- in three dimension. *Journal of Statistical Physics* 82:155–181, 1996.
- [53] Ferrenberg, A. M. and Swendsen, R. H. Optimized monte carlo data analysis. *Phys. Rev. Lett.* 63:1195–1198, 1989.